CHAPTER 3 – CASE STUDY FOR THE IMPLEMENTATION OF AN AUTOMATED ULTRASONIC TECHNIQUE TO DETECT FATIGUE CRACKS IN AIRCRAFT WEEP HOLES

3.1 Introduction

Prior work has shown the potential of a two element ultrasonic transducer technique for the generation and measurement of circumferential creeping waves around a weep hole to determine the existence of top cracks [16]. The use of both the pulse-echo and the pitch-catch responses were found to greatly increase the sensitivity of the method. From these studies, a feasible procedure was developed to detect top cracks for the dry weep hole case under laboratory conditions [16]. To implement this promising method as a robust protocol, a number of challenges had to be addressed as discussed in this Dissertation. First, the laboratory procedure requires considerable care in processing the A-scan signals for top crack detection. The creeping wave signal must be separated from the preceding specular signal and from the noise signals generated by irregular geometrical features of the structure. Second, a method to locate the weep hole and to position the transducers for bottom and top crack detection must be added to the protocol. To reduce the likelihood of operator error in conducting these tasks, an automated technique for the acquisition and classification of the signals for both bottom and top

crack detection was developed by Aldrin et al [22,23].

This chapter describes the implementation of an automated procedure from the initial proof of feasibility phase to in-field application. The tasks for implementation included the development of an automated algorithm for performing the analysis, interfacing the classification software with both the inspector and the acquisition hardware, training of the algorithms using samples closely representing field conditions, in-field validation at Warner Robins Air Logistic Center (WR-ALC), and final PoD assessment through both in-lab sensitivity studies and inspector validation at WR-ALC. Although several challenges were encountered during implementation, a robust procedure that exceeded the detection goal of 0.070 in. established at the start of the program was successfully developed and validated.

3.2 Ultrasonic Technique

The automated ultrasonic technique uses a dual transducer approach functioning in both the pulse-echo and pitch-catch modes [16]. The dual transducer probe was incorporated into an automated scanning fixture allowing for X-Y scan control on the wing surface. Figure 3.1 displays the transducer and scanning fixture. Using this scanning configuration, the automated algorithm must perform the following tasks:

- Determine the number of weep holes within the scan area,
- Determine the reference location for each weep hole,

- Determine the presence of a bottom crack for each weep hole,
- Determine the presence of a top crack for each weep hole.

Locating the weep holes can be accomplished using the C-scan amplitude data for the transducer in the pulse-echo mode. The section of the C-scan amplitude plot with the greatest root mean square value is normalized and a hill climbing technique is applied toward locating the amplitude peaks. A known minimum distance of separation of 1.0 in. exists between weep holes. If the peaks exceed a threshold and are separated by more than this minimum distance, then the amplitude signals are considered to be from weep holes. From this information, a location range for each weep hole is obtained.

Figure 3.1. View of the dual transducer probe and automated scanner system on a sample panel during the validation experiment.

A correct determination of the reference location for each weep hole is required for positioning the transducer for both top and bottom crack detection. The C-scan amplitude plot is again used for the determination of the reference location. Simultaneously, the C-scan amplitude plot in conjunction with the Full A-scan signals can be used to determine the presence of a typical bottom crack. The details of the bottom crack inspection procedure can be found in Chapter 2. The schematic for the complete bottom crack detection procedure is shown in Figure 2.2.

For top crack detection, both reflected and transmitted Rayleigh wave signals obtained from the pulse-echo and pitch-catch transducers were used in the procedure. Simulations of the scattering from weep holes by a transducer signal have been previously developed by Aldrin et al [23]. Details concerning the parameters for these simulations are presented in Appendix A. Figures 3.2(a) and 3.2(b) display contour plots of the total field response to an incident in-plane shear pulse on the weep hole for cases of no crack and top crack conditions, respectively, for four subsequent times. In both diagrams, an initial shear specular reflection of the incident shear wave is observed. In addition, the incident shear wave generates a Rayleigh wave which propagates along the surface of the weep hole. For the no-crack case, the Rayleigh wave can clearly be seen leaking energy into the riser and thus generating a significant circumferential shear wave that propagates from the hole. For the top crack case, the Rayleigh wave impinges on the base of the notch which generates a reflected Rayleigh wave propagating back from the notch. This reflected Rayleigh wave also generates a significant circumferential shear wave propagating from the hole. These plots clearly suggest the application of pulse-

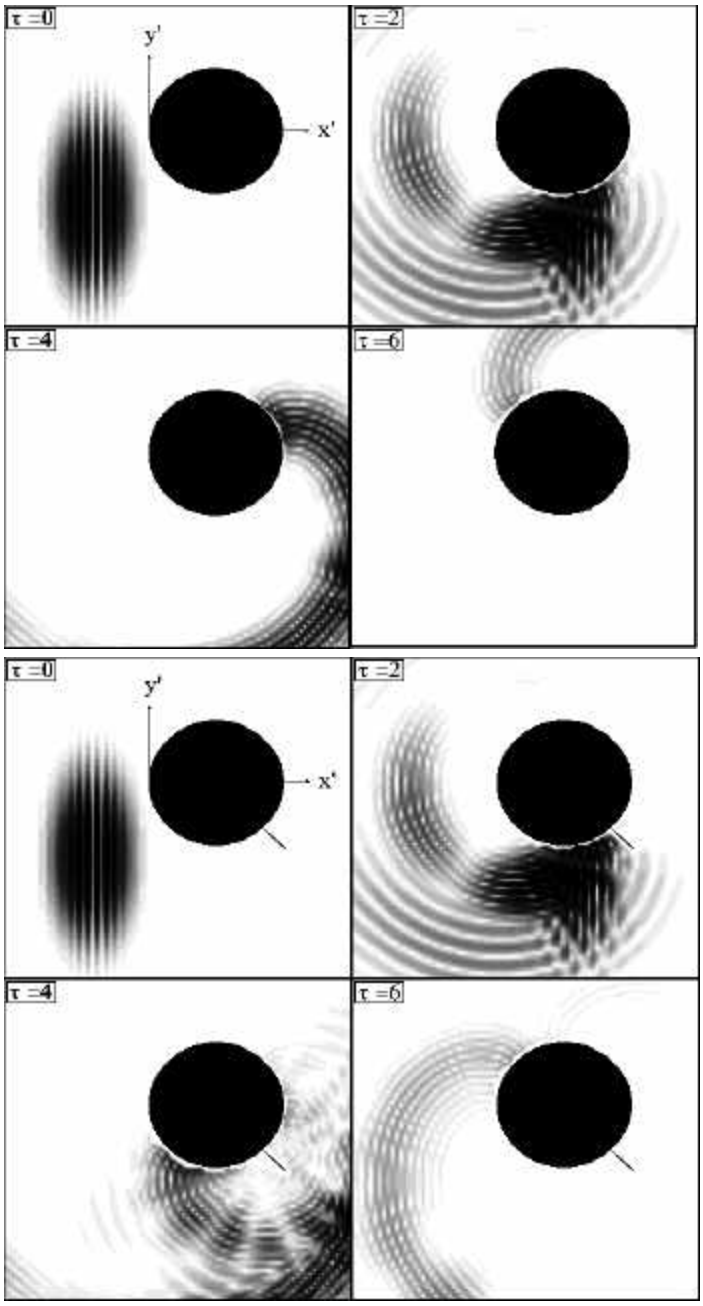

Figure 3.2. Contour plots of the total displacement field response to an incident in-plane shear pulse on a 1/4" diameter weep hole for (a) no crack and (b) with a 1.8 mm (0.070”) crack cases for four time steps, $\tau = 0,2,4,6$; $\tau = (t-t_o)*c_t/r$.

echo and pitch-catch measurements of the returning reflected and transmitted circumferential shear waves so as to best ascertain the top crack condition for the weep hole as was previously observed by Nagy et al [16].

Once these signals have been acquired, a gate is applied beyond the specular response to sift out the circumferential signal. The reference specular pulse-echo signal was used to adjust the gate location due to variation in hole depth and diameter variation. The ratio of the peak-to-peak value of the reflected signal with respect to the peak-to-peak value of the transmitted signal is used for classification purposes. Due to hole size variation, an approach using ratio values for multiple transducer locations (from a 4 step by 5 step grid) and using a neural network with 20 input nodes to classify this data set was chosen as the most robust methodology. A multilayer feedforward neural network with one hidden layer trained using backpropagation was used.

A total of 208 sample weep hole configurations were used for training. A total of 72 bottom flaw samples and 70 top flaw samples were included in the training set. The variations incorporated in the training set included crack type (sawcut notch, EDM notch, fatigue crack), crack length, combinations of top and bottom crack locations, weep hole surface condition, weep hole diameter, location near lap joint, wing surface condition, transducer positioning, transducer direction and pulser type.

Concurrent development of a C-scan based inspection technique was also pursued. Bottom crack detection was performed by inspectors viewing the pulse-echo C-scan images and assessing the existence of one or two peaks for each weep hole detected.

For top crack detection, a C-scan methodology was also developed using a surface following gate to sift out the circumferential wave signals after the initial specular signal. This approach only uses the pulse-echo signal but requires that the procedure be performed from both scan directions for robustness. This C-scan based approach was used as a baseline approach for comparison with the automated inspection procedure and as a backup approach in case the automated inspection procedure was unable to meet the design requirements.

3.3 Equipment and Operator Interface

The automated, neural network based procedure and the C-scan procedure incorporated the Ultra Image IV (UI-IV) system provided by SAIC Ultra Image International. The dual transducer probe shown in Figure 3.1 was incorporated into an automated scanning fixture with an automatic water couplant supply. For the automated procedure, the necessary data were obtained via the acquisition of the full A-scan. Scan increments of 0.020'' in both X and Y scan directions allow for good resolution for characterizing the weep hole condition. The ultrasonic transducer used in the inspection was originally developed by AFRL at Wright Patterson AFB which consists of two (2) 5 MHz, 0.250 in. diameter elements mounted on a shear wave wedge in a dual tandem configuration resulting in a 45-degree angle in aluminum. Three channels of data were acquired from the probe. The signal from the pitch transducer is split to measure both the

specular reflection from the weep hole with a lower gain setting and the reflected 'leaky' Rayleigh wave signal with increased gain. The transmitted 'leaky' Rayleigh wave signal was acquired by the catch transducer with increased gain.

The inspection of C-141 weep holes using a combined ultrasonic imaging/neural net data analysis was performed utilizing a UI-IV linked to the Neural Net Computer (NNC) via a Local Area Network (LAN). The UI-IV will gather the ultrasonic data and pass this data to the NNC via the LAN. The two computer systems are controlled by a single keyboard, video monitor, and mouse and a keyboard video monitor switch is utilized to switch these devices between the two systems.

All of the algorithms discussed have been implemented into the neural network classification software. An operator interface has also been developed for the neural network classification software for ease of use. Figure 3.3 displays a view of the interface for the weep hole classification program. The interface incorporates the following features in order to improve the speed and accuracy of the automated classification procedure:

- There are two forms of classification, Single Run and AutoDetect Run. Single Run will perform the analysis on the selected data set. AutoDetect Run first prompts the operator to select a directory to monitor, next performs the classification procedure when a new data set has been saved from the UI-IV, and continues to monitor the directory for a new data set.
- When the operator interface program is initially started, the program automatically creates a report file named using the current time and date.

Summary results are automatically saved for each analysis. This file can be viewed as a spreadsheet at a later time.

- For each run, the program checks the settings on the Ultra Image IV against required settings for weep hole classification and indicates to the operator which setting may be in error. This feature allows the operator interface to also function as an expert system.
- Upon completing each analysis, the interface displays the number of weep holes found, the locations of the weep holes, and multiple visual and numeric indicators of the neural network classification results. These displays are a means of building confidence in the performance of the automated classification software by the operator.

Approximate classification time for the program given a single weep hole case is about 20 seconds on a PC with an Intel Pentium 400c CPU.

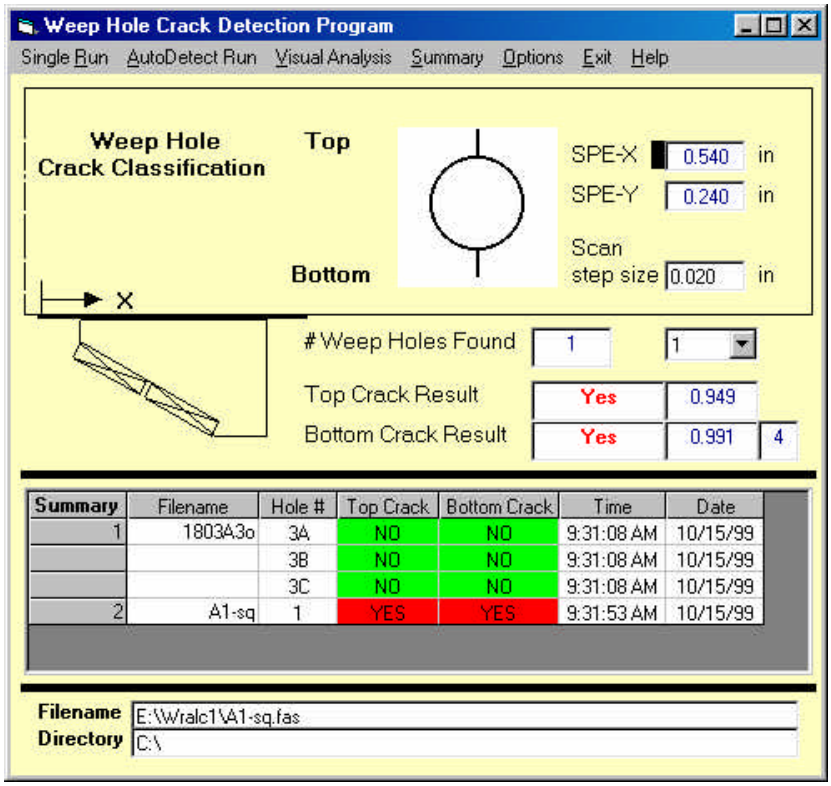

Figure 3.3. Operator interface for neural network assisted, automated classification software.

3.4 Validation Specimens

The test specimens used in the experiment were sectioned from an actual lower wing panel cutout removed from a C-141 aircraft. Seven test specimens were cut out of the panel. For this inspection process, a full-scale validation was performed with a total of 280 weep hole sites, of which 90 contain randomly distributed EDM notches of

prescribed size. The approach and results may be summarized as follows, see Aldrin et al [22]:

- Assume a target EDM notch size for 90 percent probability of detection (with a 95 percent confidence level) of 0.070 in.
- For fitting PoD curves, a uniform notch length distribution in the log scale is selected over the range of notches in which the PoD curve is effective. An estimate was made for a notch length with a 50-50 chance of being detected of a_{50} = 0.035 in., and a notch length with an extremely small chance of missing was estimated as a_h = 0.105 in., we obtained a ratio, a_h / a_{50}, of 3.
- Table 3.1 gives notch lengths uniformly spread in the log scale that are centered at a_{50} and have an upper limit of a_h for 2k + 1 points (k=1,2,3,4). A flaw size distribution with k=3 (7 points) was selected from Table 3.1 for our study. This distribution will both test the lower end capability of the inspection technique and properly validate the detection goal.
- The U.S. Department of Defense Nondestructive Evaluation System Reliability Assessment (MIL-HDBK 1823) recommends 60 notches when hit/miss data are taken and 40 notches when signal data are analyzed [41]. For this experiment, 90 notch sites were used: 30 with top notches, 30 with bottom notches, and an additional 30 holes with both top and bottom notches evenly distributed.

Table 3.2 shows the distribution of the EDM notches in the weep holes used for validation. The various weep holes were located on 7 different panels. Each panel contained 5 risers. In addition to the 89 holes represented in Table 3.2, there were an

additional 187 holes that contained no flaws. There were 21 additional weep hole sites that were not used in the analysis because of access problems or lack of accurate characterization. The neural network approach was not trained to this sample set but trained to a different set representing the expected field variation using both simulated and experimental data.

Table 3.1. Recommended Flaw Size Distribution.

Number of Points	Flaw Size Distribution			
	k=1	k=2	**k=3**	k=4
1	0.012”	0.012”	**0.012”**	0.012”
2	0.035”	0.020”	**0.017”**	0.015”
3	0.105”	0.035”	**0.024”**	0.020”
4		0.061”	**0.035”**	0.027”
5		0.105”	**0.050”**	0.035”
6			**0.073”**	0.046”
7			**0.105”**	0.061”
8				0.080”
9				0.105”

Table 3.2. Number of Inspection Sites by Flaw Size.

					Top				
Bottom	0.000”	0.012”	0.017”	0.024”	0.035”	0.050”	0.073”	0.105”	TOTAL
0.000”	187	4	4	5	4	5	4	4	217
0.012”	4	2						2	8
0.017”	4		2		1		2		9
0.024”	5			1		2			8
0.035”	4		1		2		1		8
0.050”	5			2		2			9
0.073”	4		1		1		3		9
0.105”	4	2						2	8
TOTAL	217	8	8	8	8	9	10	8	276

3.5 Field Demonstration

To fully test the inspection procedures that had been developed, on-wing demonstrations of the weep hole inspection processes were performed on a C-141 aircraft in one of the production hangars at the Warner Robins Air Logistics Center in Warner Robins, Georgia [22]. Thirteen sets of weep holes were inspected using the automated, neural network based procedure and the C-scan procedure. This inspection area was chosen because it contained painted and unpainted surfaces. The scanner was mounted both spanwise and chordwise to detect weep hole sets 2, 3, and 4. The scanner was mounted in various orientations under the wing, both spanwise and chordwise, to pick up a variety of weep holes.

Ultrasonic inspection scans were performed on both painted and unpainted skin surfaces. A total of 12 scans on the painted surfaces yielded correct calls in every instance. However, 4 scans on the stripped surfaces yielded a number of false bottom crack calls for the automated neural network procedure. In reviewing the ultrasonic signals, it was noted that the system yielded distorted signals attributed to the square wave pulsers that were on the Warner Robins UI-IV system. It was this reason that corrective action was taken by implementing the algorithm based on the spatial signal variation, as previously discussed in Chapter 2. All of the data that had been acquired to date was rerun using the modified neural net approach and correct calls were made in every case.

3.6 Laboratory and Field Validation Tests

In order to understand the inspection procedures and the possible impact of deviations from the set-up parameters, a laboratory parametric investigation was conducted, Aldrin et al [22]. In this investigation, the three factors, transducer gain, scanner skew and timebase delay, which could potentially impact the outcome of the inspection were systematically varied. An expert user, who applied the algorithms presented here to make a call, carried out the laboratory runs.

Probability of detection (PoD) curves for the laboratory runs of the inspection processes are shown in Figure 3.4. It is evident that both the neural net and C-scan processes exceed the 0.070 in. detection goal that was established at the start of the program. Two of the runs had fewer detects for the top flaws using the C-scan method. These were runs with a lower gain setting and indicate that there is some decrease in reliability for the C-scan method with the falling of gain. However, the same decrease is not observed when the neural net process is used. Due to its robustness to variation in gain, the neural net process reliably detected smaller flaws than the C-scan process. The number of false calls for the neural net on the top flaws increased from a rate of 1.0% (9 false calls) to a rate of 1.4% (13 false calls), not a significant change.

To determine the reliability of the inspection process when implemented in a field environment, an experiment was designed to address the issues of inspector experience and training, the inspection environment, and normal operating conditions [22]. Four

inspectors at Warner Robins were chosen to inspect the panels without knowledge of the flaw placements. Three of these inspectors, who were from the population denoted LJ, had prior experience with the Ultra Image IV (or similar) equipment and had significant experience in the field testing environment. One inspector was from the population denoted TI. This inspector was familiar with the operation of the Ultra Image IV, but had limited field testing experience. All four inspectors received training on the new procedures, and all were asked to perform the inspection using both the C-scan and the neural net algorithm procedures. One of the LJ inspectors completed an inspection using the neural net algorithm, but did not complete the inspection using the C-scan method. The result was three completed regular C-scan and four completed neural net inspections.

The probability of detection curves for the top crack calls and the bottom crack calls are shown in Figures 3.5 and 3.6, respectively. The 2-parameter PoD curves were fit to the data gathered in the field. Although the detection rates were high, a few missed calls at larger crack lengths resulted in irregularity for some PoD curves. In both Figures 3.5 and 3.6, it should be remembered that the smallest flaw size is 0.012 in. Therefore, the sharp decreases around 0.010 in results from only a few of the smallest flaws being missed. The curves of Figures 3.5 and 3.6 show that the neural net approach is achieving the desired level of detection. The significant reduction in variability between inspectors in making classification calls with the use of the neural net approach is an additional desirable result.

3.7 Summary and Discussion

Tables 3.3 and 3.4 summarize the flaw sizes having a 90% probability of detection and the false call rate from the PoD validation study for the two approaches. The application of the neural net assisted automated inspection approach significantly increased the detectability of smaller top and bottom cracks, with the largest impact on the detection of top cracks. This increase in detectability did not produce an increase in the false call rate, but to the contrary, reduced the false call rate significantly for top crack detection. In addition, the automated neural network approach only requires scanning from one direction while the C-scan approach requires scanning from both directions. Thus, the automated neural network approach provides a significant improvement in both detectability and inspection time over the C-scan approach.

The validation effort for the ultrasonic inspection of the C-141 weep holes was carried out using fabricated samples containing EDM notches. There is always a question as to the correspondence between signals from artificial flaws and actual flaws. Therefore, there is no claim that the reliability figures given here map directly into what is achievable in the field. However, the present study establishes that the inspection procedure is capable of finding small flaws.

Table 3.3. Summary of PoD Validation Results for C-Scan Approach

	Top Crack	Bottom Crack
PoD (90%)	0.045 in.	0.024 in.
False Call Rate	1.4 %	1.6%

Table 3.4. Summary of PoD Validation Results for Neural Network Approach

	Top Crack	Bottom Crack
PoD (90%)	0.020 in.	0.010 in.
False Call Rate	0.1 %	1.1%

The PoD results shown in Figures 3.4 – 3.6 provide quantitative inspection data that will allow the C-141 structural managers to make informed decisions about the implementation of the new weep hole inspection process. When fully implemented by WR-ALC, this will be the first successful NDI production application of an automated classification technique using neural network technology by the Air Force. A key contributor to the success of neural networks for this case was the use of expert knowledge gained through simulated and experimental studies to design the algorithms such that the complexity of the data that the neural networks must properly classify was minimized. At present, plans are to replace the eddy current weep hole inspection with the neural-net enhanced ultrasonic weep hole inspection technique. Except for back-up inspection to validate neural net crack calls, the new weep hole technique will essentially eliminate inspector fuel tank entry requirements. It is estimated that the new technique will reduce the current man-hour requirements for eddy current inspection by almost one-

half. The first production aircraft is planned to be inspected in early FY01, Aldrin et al [22].

The need for a focused multi-disciplinary team must be mentioned as important toward the success of developing and implementing an automated inspection procedure. Expertise in experimental design is important to successfully obtain the necessary data for a proper PoD validation within the allotted time and cost constraints. In addition, a broad range of experience must be gained with an automated procedure in order to guarantee its robustness not just for an in-lab demonstration, but for the wide variety of variation expected over the life of its use in the field.

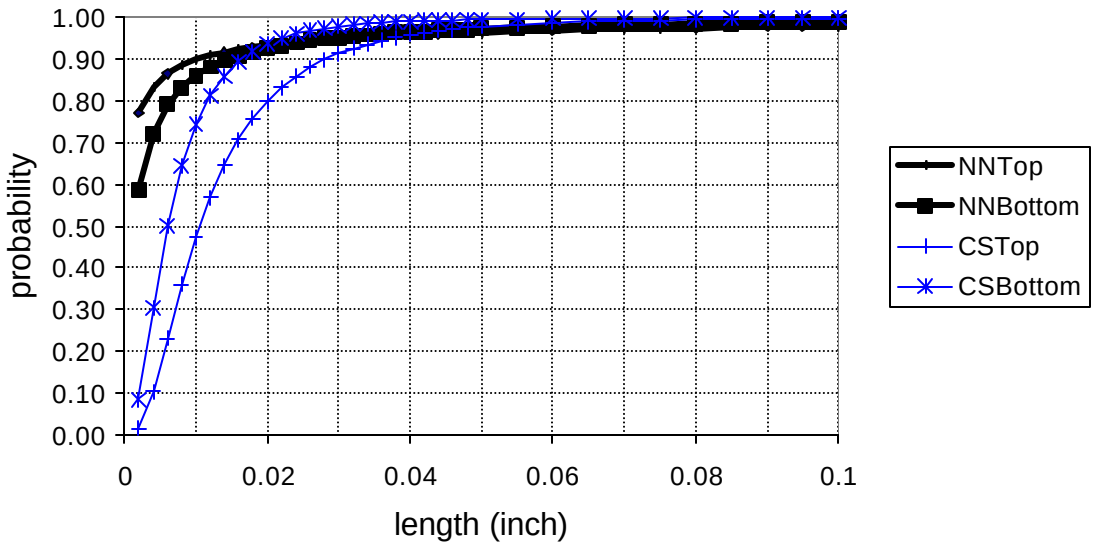

Figure 3.4. Laboratory probability of detection results using neural network assisted (NN) and C-scan (CS) classification approaches for top crack (Top) and bottom crack (Bottom) detection.

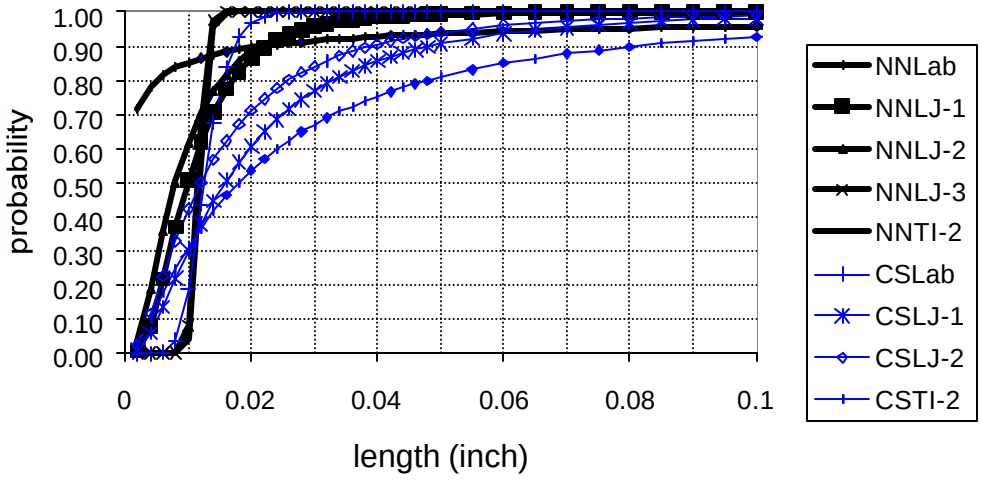

Figure 3.5. Top flaw probability of detection using neural network assisted (NN) and C-scan (CS) classification.

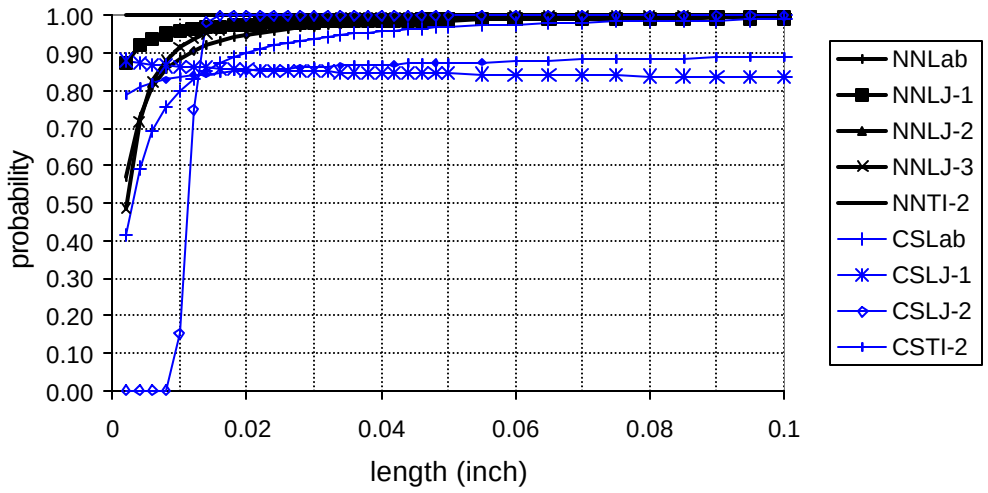

Figure 3.6. Bottom flaw probability of detection using neural network assisted (NN) and C-scan (CS) classification.